Advances in Science and Technology Research Journal

Advances in Science and Technology Research Journal, 2025, 19(6), 291–300
https://doi.org/10.12913/22998624/202860
ISSN 2299-8624, License CC-BY 4.0

Received: 2025.02.17
Accepted: 2025.04.15
Published: 2025.05.01

Sintered steels intended for fabrication of metal-diamond composites

Joanna Maria Borowiecka-Jamrozek[1*], Janusz Stefan Konstanty[2]

[1] Faculty of Mechatronics and Mechanical Engineering, Kielce University of Technology, al. Tysiąclecia Państwa Polskiego 7, Kielce, Poland
[2] Faculty of Metals Engineering and Industrial Computer Science, AGH - University of Krakow, al. Mickiewicza 30, 30-059 Krakow, Poland
* Corresponding author's e-mail: jamrozek@tu.kielce.pl

ABSTRACT

The main objective of the present work was to determine a high-alloy Cu-Sn-Ni steel powder preparation conditions and as-consolidated properties of the material in view of its application as a matrix in metal-bonded diamond tools. A mixture of three commercial powders was subjected to ball milling for 30, 60 and 120 hours and then consolidated by the hot-press route. The sintered specimens were tested for density, hardness and oxygen content, and subjected to static tensile test, dilatometric measurements and microstructural observations. The results obtained indicate that the tested material shows relatively high density, hardness and mechanical strength and thus lends itself to manufacturing of diamond-impregnated tool components used for processing of natural stone and ceramics.

Keywords: powder metallurgy, sintered diamond tools, metallic matrix, mechanical properties, dilatometry.

INTRODUCTION

Nowadays diamond saw blades and grinding tools are commonly used for processing natural stone and ceramics. The cutting/grinding segments consist of synthetic diamond grits embedded in a metallic matrix. The segments are exclusively manufactured by powder metallurgy (P/M) technology. Metals commonly employed in various matrix systems are cobalt, iron, copper, tin, tungsten and nickel [1–4] with cobalt being most often used in the past [2, 5–7]. Recently, a growing application of inexpensive premixed and ball milled iron-based powders has been observed [8–16]. It has been found that inexpensive metallic matrices containing iron, copper, nickel and tin can be easily consolidated to near-full density at relatively low temperatures, far below 1000 °C, and show desired as-sintered mechanical properties comparable to those of hot pressed cobalt [10, 11, 14, 17, 18]. One important role of the matrix is to firmly hold diamond crystals on the working face of the tool. Therefore it is advantageous when the matrix has a markedly greater thermal expansion coefficient compared to diamond in order to shrink clamp diamond crystals in the matrix on cooling from the consolidation temperature [3, 19–22]. In addition, the matrix material should also combine high hardness and yield strength with good ductility [1–4, 19, 23–28].

MATERIALS AND METHODS

Powders

Based on the results previous research [2], an experimental iron-based powder was designed and obtained from the following commercial powders:

- carbon reduced iron powder with particle sizes ranging from 20 to 180 μm,
- fine carbonyl nickel powder with an average particle size (Fisher number) of 2.4 μm,
- atomised bronze powder containing 15% tin, with particle sizes below 45 μm.

The starting powders are shown in Figure 1. The starting mixture of 28% tin bronze (23.8% Cu and 4.2% Sn), 12% nickel and the balance iron was made by mixing in a Turbula-type mixer for 30 minutes and subjected to prolonged milling in the EnviSense RJM-102 laboratory ball mill in ethyl alcohol. The milling vial was filled to 50% of its volume with 100Cr6 steel balls 12 mm in diameter. The milling times were 30, 60 and 120 hours.

After milling the powders were analysed for apparent density and tap density using procedures standardised in ISO 3923-2 [29] and ISO 3953 [30], respectively. The Scott volumeter method was used to determine the apparent density because the ball milled powders did not flow through the 2.5 mm orifice Hall funnel. Both the premix and all ball milled powders were also subjected to particle size analysis using the coherent light scattering technique. The particle size distributions (PSDs) were estimated by means of the HELOS (H2769) & RODOS laser analyzer and the WINDOX 5 software programmed to measure particles from 0.1 to 2000 μm.

Powder consolidation

The ball milled powders were consolidated by hot pressing in graphite moulds using the Idea Unidiamond (Italy) press. By using moulds with multiple cavities it was possible to simultaneously hot press four rectangular specimens ~7 by 12 by 40 mm in size. All ball milled powders were kept at 900 °C at 35 MPa for 3 minutes. Detailed information on the pressing cycle is shown in Figure 2.

Measurements of physical chemical and mechanical properties

Evaluation of as-sintered densities was carried out based on the Archimedes' principle. The oxygen content was measured using the LECO RO-416 instrument. The Vickers hardness was determined at a 9.81 N load using the Innovatest Nexus 4000 hardness tester. The hardness numbers were obtained by averaging ten readings on each specimen. The static tensile test was carried out with the use of a universal testing machine type UTS-100 with data recording system provided by Zwick. Tensile properties, such as tensile strength (R_m), 0.2% offset yield strength ($R_{0.2}$) and elongation (ε), were determined on flat test pieces machined to obtain the gage length of 20 mm and gage cross section of 6.5 by 11.3 mm.

Phase analysis (X-ray diffraction)

The phase analysis of as-consolidated specimens was performed using the X-ray diffraction (XRD) technique. The PANalytical Empyrean

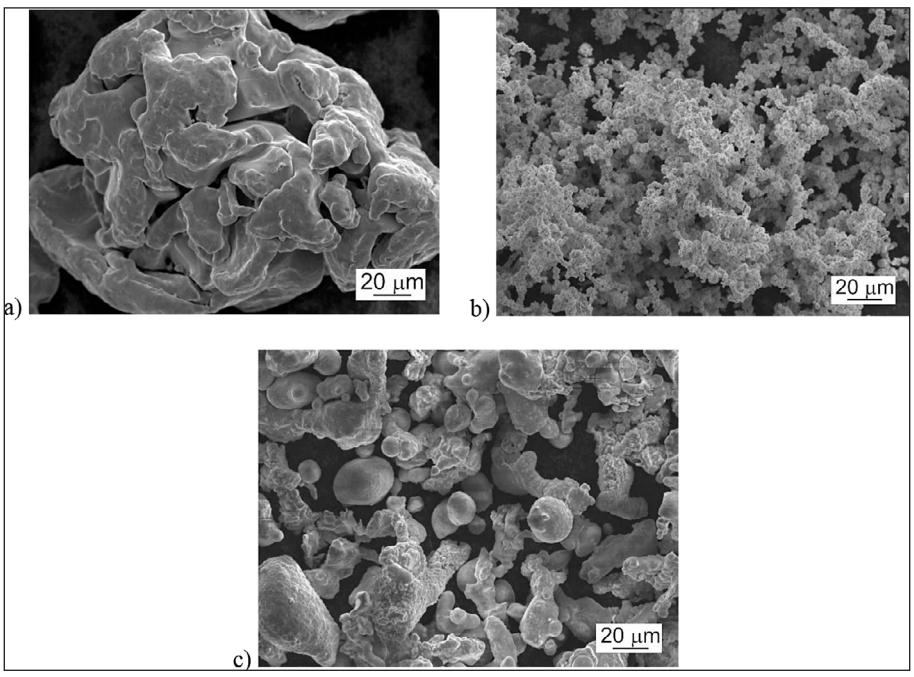

Figure 1. Scanning electron micrographs of the starting powders: (a) carbon reduced iron, (b) carbonyl nickel, (c) atomised tin bronze

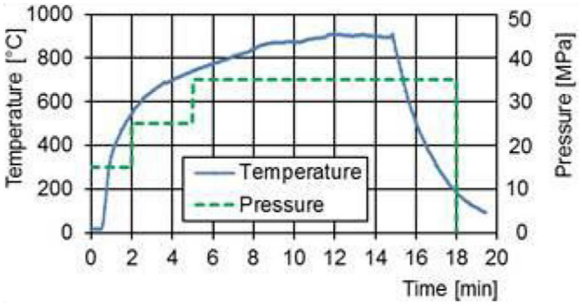

Figure 2. Typical temperature/pressure versus time plots

diffractometer fitted with PIXcel detector was using x-rays emitted from a copper target (K-α_1 line, $\lambda = 1{,}5406$ Å).

Dilatometry

The high-temperature Netzsch DIL-402-E dilatometer was used to determine the dimensional changes of the as-consolidated matrix materials during heating to 950 °C in argon. Prior to testing, the hot pressed specimens were machined to 15 by 5 by 5 mm in size.

Microstructural studies

Metallographic and fractographic observations of microstructure in the hot pressed specimens were carried out using the JSM-7100F scanning electron microscope fitted with the EDS X-Max-AZtec X-ray microanalysis system from OXFORD INSTRUMENTS.

RESULTS AND DISCUSSION

The evolution of powder morphology with the time of milling is presented in Figure 3.

The flaky shape characteristics of the ball milled powders impair their flowability and adversely affect apparent density and tap density. The results given in Table 1 show a marked decrease in both densities when milling time is extended from 60 to 120 hours. In addition to the change of particle shape (flaking), ball milling directly affects the particle size and particle size distribution of the powder. The graphical representation of the PSDs is shown in Figures 4 and 5.

From the results of Figures 4 and 5 it is evident that the bimodal PSD of the powder mix changes to the unimodal one that shifts toward narrower size range with milling time. The original shape of the powder mix (Fig. 1) is altered by ball milling to form irregularly shaped particles, which retain the flake-like morphology even after prolonged milling extended to 120 hours (Fig. 3). After consolidation all specimens were subjected

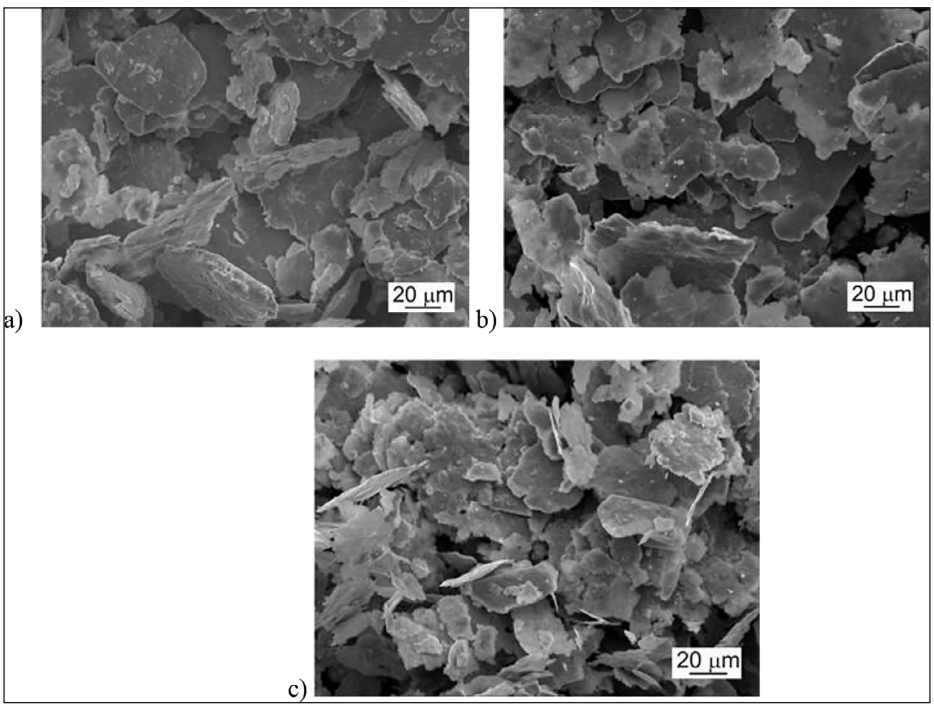

Figure 3. Effect of milling time on particle shape and size: (a) 30 hours, (b) 60 hours and (c) 120 hours

Table 1. Apparent densities and tap densities of ball milled powders

Powder milling time [hours]	Apparent density [g/cm³]	Tap density [g/cm³]
30	0.63	1.25
60	0.62	1.14
120	0.46	0.93

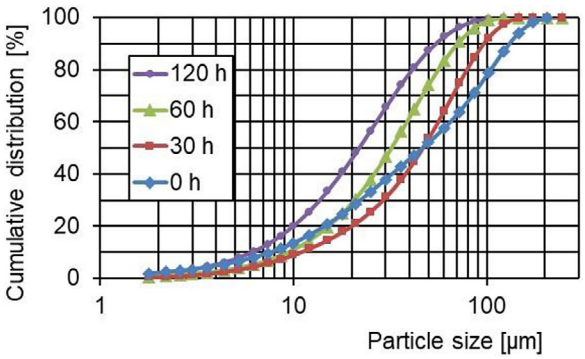

Figure 4. Cumulative plot of particle size distributions

to density measurements and hardness tests. Selected specimens were also tested for oxygen content. The results are presented in Table 2.

As seen in Table 2, prolonged milling leads to excessive pickup of oxygen by the powder, which results in lower as-sintered density and hardness of the material. Initially hardness rises but abruptly falls when milling time is increased from 60 to 120 hours. Similar trend is observed in the static tensile test results. Fig. 6 and Table 3 illustrate a marked rise in 0.2 offset yield strength and tensile strength at the expense of reduced ductility (elongation) as milling time increases from 30 to 60 hours. Thereafter all these properties are mildly reduced.

The phase analysis results of as-consolidated specimens are presented in Figures 7 and 8. From Figure 8 it is evident that the material consolidated from premixed powders is mostly composed of (αFe) and (Cu) phases. The Cu 111 and 200 peaks, located at 43.295 and 50.431°, respectively, are shifted to lower angles because of tin dissolved in copper. The (Cu) 111 peak is asymmetic due to the overlapping (γFe) 111 component as illustrated in Figure 9. The retained austenite can be mostly attributed to the stabilizing effect of nickel. The absence of nickel peaks implies complete dissolution of fine nickel particles in iron and molten bronze during hot pressing at 900 °C. The volume fraction of austenite in the iron phase can readily be calculated by inserting the XRD data from Figure 9 into the following equation:

$$V_{austenite} = \frac{1.4\, I_{111}}{(I_{110} + 1.4\, I_{111})} \cdot 100\% \qquad (1)$$

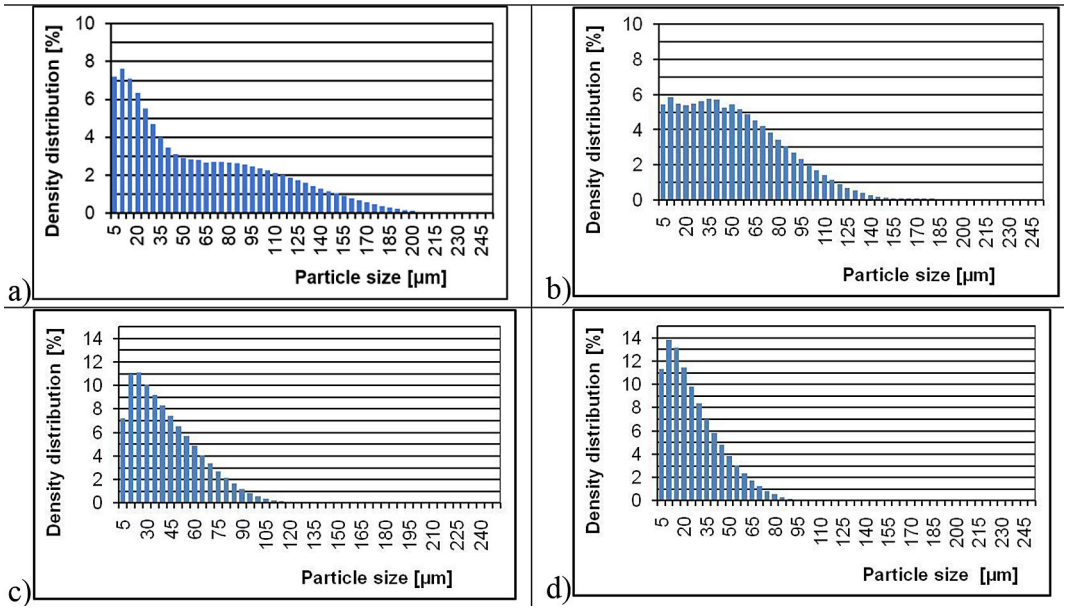

Figure 5. Size frequency distribution plots for (a) the premixed and ball milled powders for (b) 30 hours, (c) 60 hours, (d) 120 hours

Table 2. Densities, Vickers hardness numbers and oxygen contents of as-consolidated materials

Powder milling time [hours]	Density* [g/cm^3]	HV1*	Oxygen content* [wt.%]
30	8.01 ± 0.09	273 ± 15	0.59 ± 0.03
60	8.01 ± 0.05	402 ± 30	0.71 ± 0.12
120	7.91 ± 0.07	334 ± 30	0.89 ± 0.09

Note: * scatter intervals were estimated at 90% confidence level.

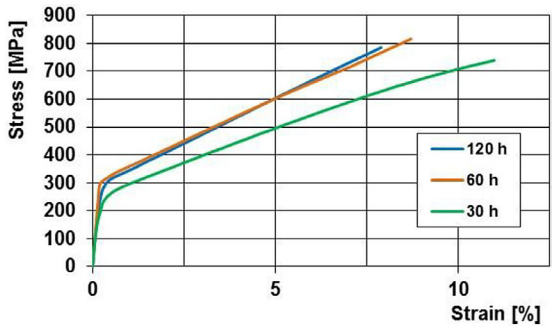

Figure 6. Representative tensile test curves

where: I_{111} and I_{110} are the integrated intensities of the {111} and {110} diffraction lines for (γFe) and (αFe), respectively.

The volume fraction of austenite in the material obtained from the premixed powders was estimated at 42% and hence the (αFe) to (γFe) ratio was around 1.38.

For the materials consolidated from ball milled powders the intensities of (γFe) peaks markedly increase at the expense of both (αFe) and (Cu) peaks. The (αFe) peaks are barely visible, although asymmetry on the right side of the (γFe) 111 peak indicates some retention of ferrite in the hot pressed specimens.

This has been confirmed by the dilatometer test carried out on the material made of the powder milled for 60 hours. The dilatometer curve shown in Figure 10 deviates from linearity between 450 and 620 °C, and above around 730 °C. The average value of thermal expansion coefficient (α) at 50–450 °C is relatively high (α=20.5·10^{-6} K^{-1}). Between 450 and 620 °C α markedly drops due to the αFe → γFe phase transformation and raises

Table 3. Results of the static tensile test

Powder milling time [hours]	0.2% offset yield strength* [MPa]	Tensile strength* [MPa]	Elongation* [%]
30	273 ± 35	739 ± 60	11.0 ± 1.4
60	330 ± 29	817 ± 32	8.6 ± 0.5
120	320 ± 44	785 ± 47	7.9 ± 1.0

Note: * scatter intervals were estimated at 90% confidence level.

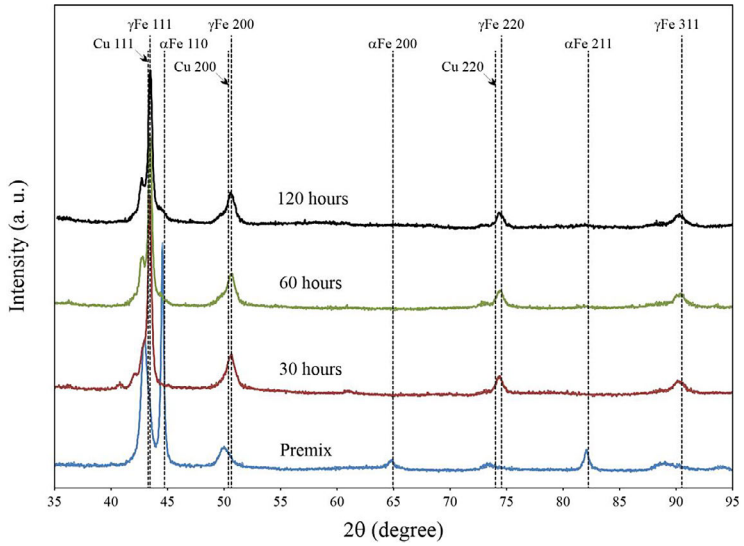

Figure 7. XRD patterns for specimens made from the premixed and ball milled powders

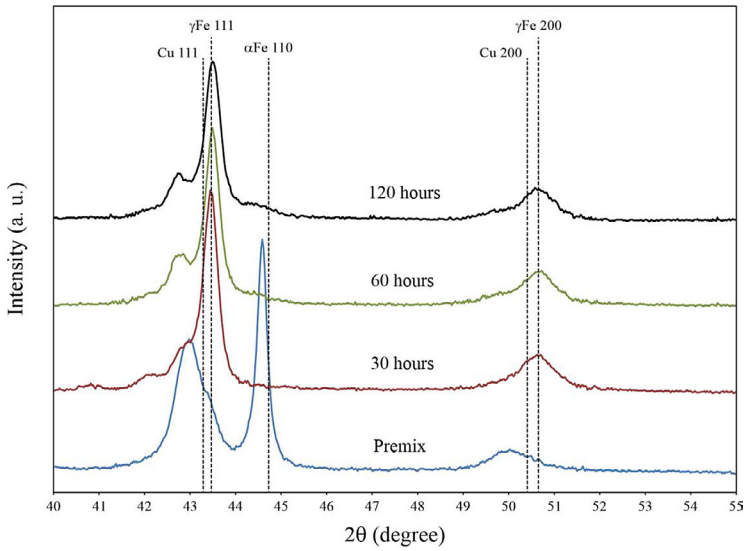

Figure 8. Magnified view of the 40–55° 2θ range of Figure 7

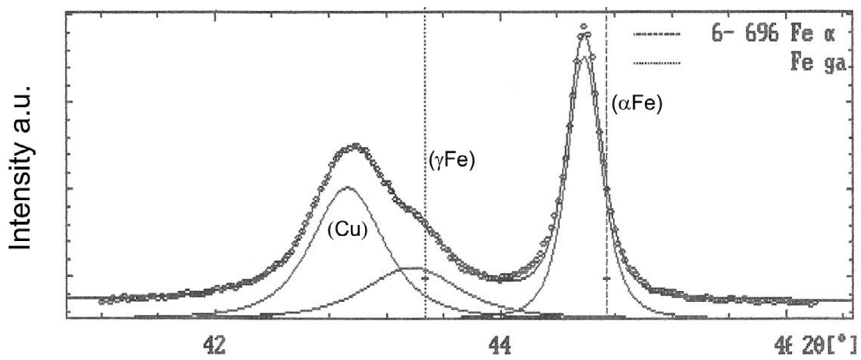

Figure 9. XRD data obtained from the specimen made of premixed powders. The observed peak shapes are shown as the sum of numerically computed components

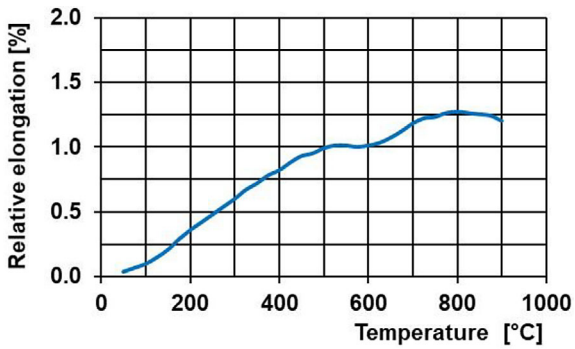

Figure 10. Dilatometer curve of dimensional changes in the material made of powder ball milled for 60 hours

again to reach the maximum value of $22 \cdot 10^{-6}$ K^{-1} at 700°C. Above 750 °C the specimen becomes softened, partly melted and distorted by the push-rod pressure. The presence of ferrite in the material made of the powder milled for 60 hours was confirmed using the peak profile fitting approach. The peak intensities from Figure 11 inserted into Equation 1 indicate that the iron phase is composed of 94% austenite and 6% ferrite. The effect of powder milling on microstructure of hot pressed specimens is shown in Figure 12. From Figure 12, it can be seen that the microstructure of the material made from the premixed powder differs from the others in that there is a clearly visible bright phase within the (Cu) phase region. The energy-dispersive spectrometry (EDS) data in Figure 13 allow to identify it as the $(Cu,Ni)_3Sn$ phase.

Additional data obtained from the Thermo-Calc software calculations using the SGTE Alloy Solutions v5.0 database indicates that a bcc $(Cu,Ni)_3Sn$ phase, equivalent to $CuNi_2Sn$, is thermodynamically stable above 443 °C. On cooling it undergoes transformation into $Cu_3Ni_{27}Sn_{10}$ through a complex multi-phase reaction. The Cu/Ni ratio in the bcc $(Cu,Ni)_3Sn$ phase increases

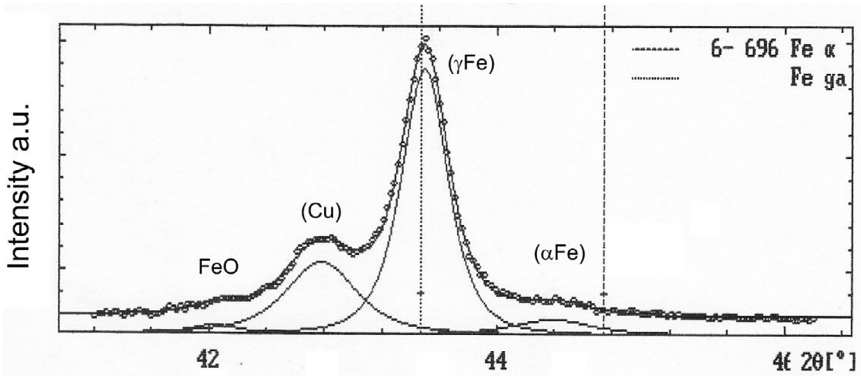

Figure 11. Numerically profile fitted XRD data obtained from the specimen made of powders milled for 60 hours

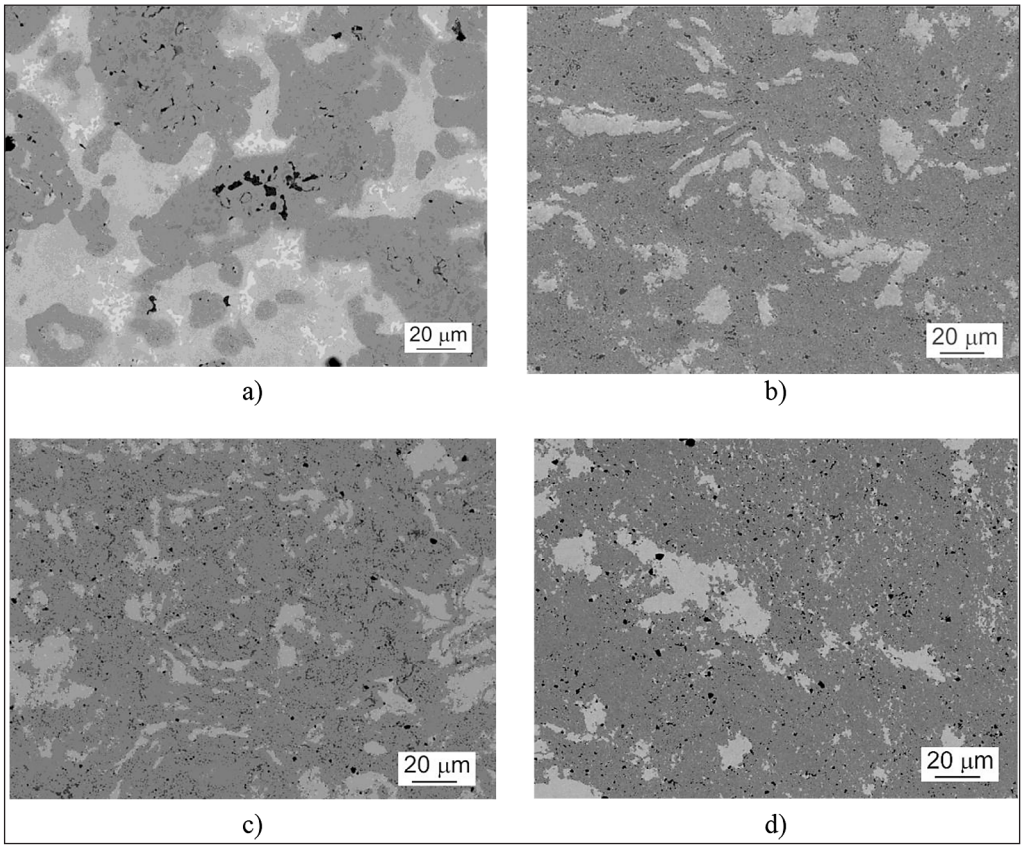

Figure 12. Microstructure of materials made from (a) the premixed and ball milled powders for (b) 30 hours, (c) 60 hours, (d) 120 hours

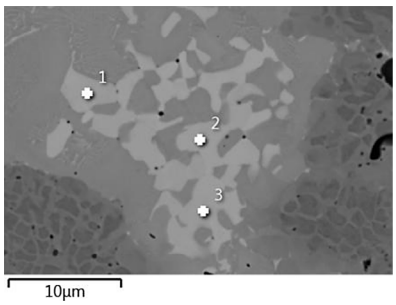

	Fe		Cu		Sn		Ni	
	wt.%	at.%	wt.%	at.%	wt.%	at.%	wt.%	at.%
1	1.6	2.1	28.2	33.2	38.5	24.2	31.7	40.4
2	2.0	2.7	29.3	34.0	36.0	22.4	32.7	41.0
3	2.3	3.1	26.2	30.6	38.1	23.9	33.4	42.4

Figure 13. Magnified view of a region containing the bright phase and the EDS analysis data

with temperature and reaches the experimental values given in Figure 13 at around 525 °C.

The microstructural observations show that the thermodynamically justified $CuNi_2Sn \rightarrow Cu_3Ni_{27}Sn_{10}$ transformation does not occur and the phase composition does not markedly change on cooling below 525 °C after hot pressing the premixed powders at 900 °C. Interestingly, from the Thermo-Calc software calculations it appears that the ferrite to austenite ratio is around 3/2 at 525 °C. Hence, the computer generated data and the dual-phase iron-rich region seen in Fig. 14 also confirm that ferrite (dark grey phase) prevails over austenite in the material consolidated from the premixed powder. The phase composition of the investigated material seems to be governed by the distribution of the nickel. During consolidation of the premixed powder the 3 min hold at 900 °C is too short for the nickel atoms to diffuse to the central parts of the coarse iron particles. Instead, the fine nickel particles readily dissolve in the partially melted bronze thereby promoting formation of $(Cu,Ni)_3Sn$. The chemical maps of elements given in Figure 15 support this reasoning, showing similarities between the distributions of nickel and tin. The application of high energy ball milling to a mix of powders enables solid-state blending of its components and altering the powder particles characteristics, with increased density of the crystal structure defects being the most important variable. Both the reduced interdiffusion distances and severe plastic deformation of the powder, that provides high diffusivity paths (dislocations), combine to enable rapid diffusion of the nickel to the iron even on heating to the hot pressing temperature. This, in turn, effectively stabilises austenite on cooling as it is evident from the results of Figured 7 and 8.

From Figure 16, it can be seen that the areas occupied by iron and nickel overlap. Contrary to the images in Figures 13 and 15, both the $(Cu,Ni)_3Sn$ phase inclusions and similarities between the distributions of nickel and tin are barely observable.

Selected EDS analysis results showing chemical compositions of phases contained in the material made from the ball milled powder are presented in Figure 17. The dark grey oxide phase visible in the microstructure (area 4) has been identified by XRD (see Figure 11) as wustite (FeO).

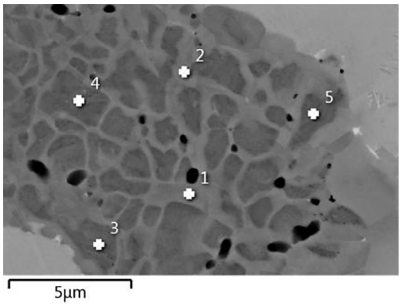

	Ni	Cu	Sn	Fe
	wt.%	wt.%	wt.%	wt.%
1	28.5	14.9	1.0	bal
2	31.7	16.2	1.2	bal
3	5.1	1.0	0.3	bal
4	2.7	1.9	0.0	bal
5	3.1	1.7	0.2	bal

Figure 14. Magnified view of a region containing the iron-rich phase and the EDS analysis data

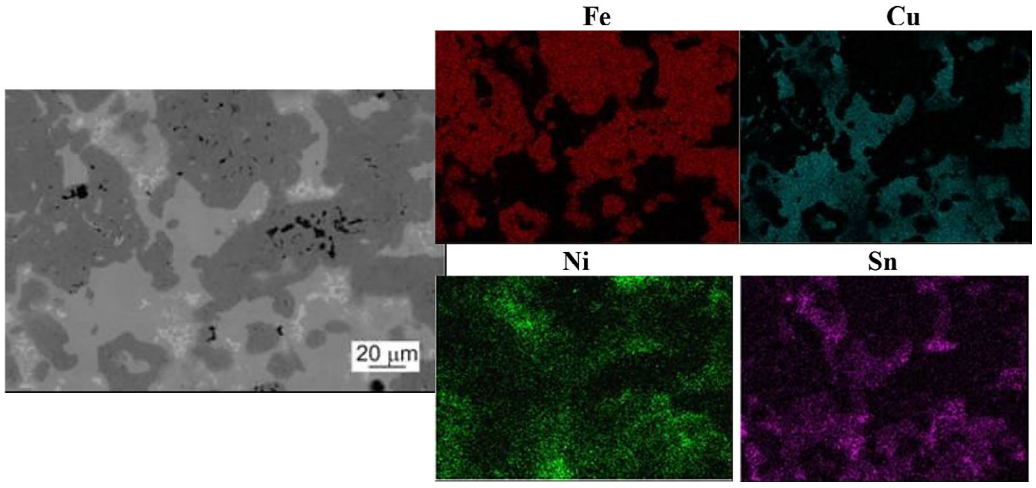

Figure 15. Elemental mapping of a specimen made from the premixed powder

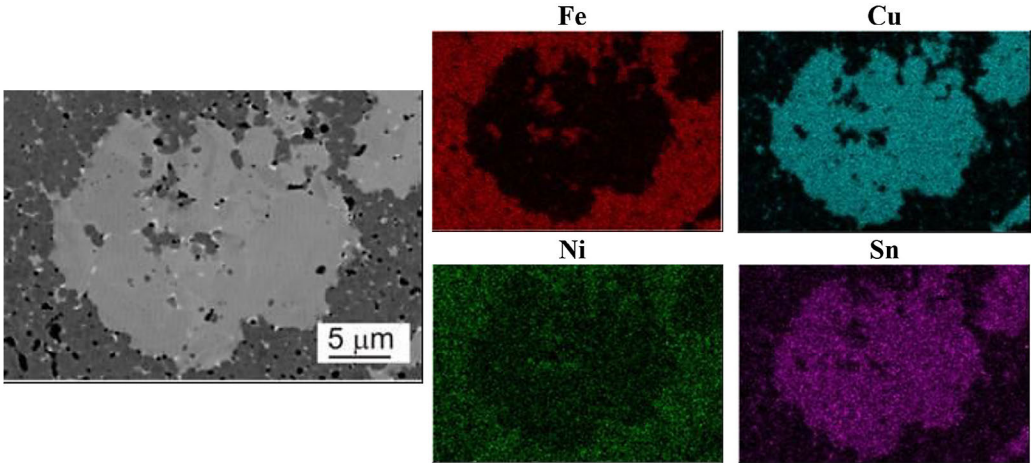

Figure 16. Elemental mapping of a specimen made from the powder ball milled for 60 hours

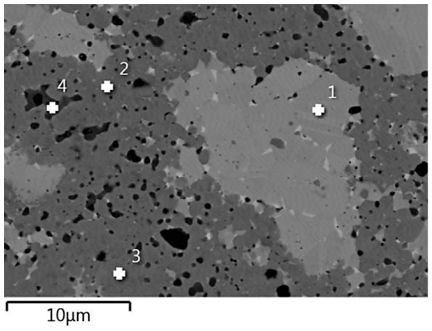

	Ni	Cu	Sn	Fe	O
	wt.%	wt.%	wt.%	wt.%	wt.%
1	5.4	bal	11.1	5.6	-
2	19.6	10.2	1.2	bal	-
3	18.7	10.3	1.1	bal	-
4	8.9	1.3	0.5	bal	17.4

Figure 17. SEM micrograph of a specimen hot pressed from the ball milled powder and results of chemical analysis performed at selected microareas

CONCLUSIONS

The results of the current study show that the ball milled high-alloy steel powders can easily be consolidated to near-full density by hot pressing for 3 minutes at 900 °C and 35 MPa. In as-consolidated condition they exhibit the required combination of relatively high hardness (> 273 HV1), yield strength (> 273 MPa) and tensile strength (> 739 MPa) with good ductility. All these properties make them suitable for the fabrication of diamond tool components (e.g., diamond segments for saw blades and grinding wheels) by the hot-press route.

For best results, the powder mix should be ball milled for around 60 minutes, during which time a satisfactory degree of particle refinement, blending of the composite structure and cold working is achieved. This ensures the highest as-sintered density (8.01 g/cm^3), hardness (402 HV1), yield strength (330 MPa) and tensile strength (817 MPa) with sufficient tensile elongation exceeding 8%. As milling proceeds over an extended time (120 hours) the oxygen content of the powder abruptly increases from 0.71 to 0.89%, whereas its apparent and tap densities are markedly decreased to unacceptable levels of 0.46 and 0.93 g/cm^3, respectively, which makes the powder difficult to handle.

At room temperature the composite microstructure of the material consolidated from ball milled powders is mainly composed of austenite and (Cu). Both these phases exhibit higher linear coefficients of thermal expansion as compared to ferrite. Hypothetically it should increase the gripping forces acting on the diamond after cooling the metal-diamond composite from the hot pressing temperature and thus improve the matrix capacity for diamond retention. From both the technical and economic point of view the composite powder produced by ball milling of the starting powders for 60 hours has been found to be most suitable for binding diamond crystals in sintered diamond tool components.

Acknowledgements

The authors gratefully acknowledge Krzysztof Chrusciel of AGH University of Krakow for his able assistance with XRD documentation. The work was supported by Kielce University of Technology and AGH University of Krakow through contracts SUBB.MKMT.24.001-01.0.10.00/1.02.001 and 16.16.110.663, respectively.

REFERENCES

1. Konstanty, J, The materials science of stone sawing. Industrial Diamond Review 1991; 542: 27
2. Konstanty, J, Cobalt as a matrix in diamond impregnated tools for stone sawing applications, 2nd Edition. AGH Uczelniane Wydawnictwa Naukowo-Dydaktyczne, Krakow 2003.
3. Konstanty, J, Powder Metallurgy Diamond Tools, Elsevier, Oxford 2005.
4. Borowiecka-Jamrozek, J, Engineering Structure and Properties of Materials Used as a Matrix in Diamond Impregnated Tools, Archives of Metallurgy and Materials 2013; 58(1): 5–8.
5. Konstanty, J, Hard tooling. Cobalt is a diamond's best friend, Cobalt News 1993; 2: 3.
6. Konstanty, J, Cobalt and Diamond Tooling, Proc. Cobalt Conference, Hong Kong, 23–24 April 1997.
7. Vliegen, J, Mishra, P, Kamphuis B-J, The use of fine cobalt powders in bonding applications, Proc. The Cobalt Conference, Hong-Kong, November 19–20, 2003.
8. Konstanty, J, Tyrała, D, Radziszewska, A, Iron-Base Materials Manufactured from Premixed Powders by the Hot Press Process, *Archives of Metallurgy and Materials*, 2009; 54: 1051–1058.
9. Barbosa, AP, et al. Structure, microstructure and mechanical properties of PM Fe–Cu–Co alloys, *Mater Des* 2010; 31: 522–526.
10. Konstanty, J, Stephenson, TF, Tyrala, D, Novel Fe-Ni-Cu-Sn matrix materials for the manufacture of diamond-impregnated tools, *Diamond Tooling Journal*, 2011; 2: 26–29.
11. Romanski, A, Konstanty, J, Ball-milled Fe-Ni and Fe-Mn matrix powders for sintered diamond tools, *Archives of Metallurgy and Materials*, 2014; 59: 189–193.
12. Konstanty, J, New highly sinterable iron-base powders for diamond wire beads, *Diamante Applicazioni & Tecnologia*, 21 2015; 82: 18–19.
13. Oliveira, FAC, Anjinho, CA, PM materials selection: The Key for Improved Performance of Diamond Tools, *Metal Powder Report* 2017; *72*: 339–344.
14. Konstanty, JS, Baczek, E, Romanski, A, Tyrala, D, Wear-resistant iron-based Mn-Cu-Sn matrix for sintered diamond tools, *Powder Metallurgy*, 2018; 61: 43–49.
15. Borowiecka-Jamrozek, J, Konstanty, J, Lachowski, J, The application of a ball-milled Fe-Cu-Ni powder mixture to fabricate sintered diamond tools. *Archives of Foundry Engineering*, 2018; 18: 5–8.
16. Konstanty, J, Tyrala, D, Easily Sinterable Low-Alloy Steel Powders for P/M Diamond Tools, *Metals*, 2021; 11(8): 1204.
17. Mechnik, VG, et.al., A study of the microstructure of Fe-Cu-Ni-Sn and Fe-Cu-Ni-Sn-VN metal matrix for diamond-containing composites, *Mater Charact* 2018; *146*: 209–216.
18. Mechnik,VG, et al., Influence of diamond–matrix transition zone structure on mechanical properties and wear of sintered diamond-containing composites based on Fe–Cu–Ni–Sn matrix with varying CrB2 content, *Int J Refract Hard Met* **2021**; 100.
19. Konstanty, J, de Chalus PA, Diamond Tooling. Stone Cutting, *Cobalt News* 1996; 4: 12.
20. Romanski, A, Lachowski, J, Konstanty, J, Diamond retention capacity: evaluation of stress field generated in a matrix by a diamond crystal, *Industrial Diamond Review* 2006; 3: 43–45.
21. Borowiecka-Jamrozek J, Lachowski J, Modelling of retention of a diamond particle in matrices based on Fe and Cu, *Procedia Engineering*, 2017; 177: 289–296.
22. Borowiecka-Jamrozek J, Lachowski J, A Thermomechanical Model of Retention of a Diamond Particle in Matrices Based on Fe, *Defect and Diffusion Forum* 2020; 405: 48–53.
23. Zaitsev, AA, et al., Development and application of the Cu–Ni–Fe–Sn based dispersion-hardened bond for cutting tools of superhard materials, *J Superhard Mater* 2012; 34: 270–280.
24. Mechnyk, VA, Diamond–Fe–Cu–Ni–Sn composite materials with predictable stable characteristics, *Mater Sci* 2013; 48: 591–600.
25. Sidorenko, DA, et al., Interaction of diamond grains with nanosized alloying agents in metal–matrix composites as studied by Raman spectroscopy, *Diam Relat Mater* 2013; 38: 59–62.
26. Mechnik, VA, Production of diamond−(Fe−Cu−Ni−Sn) composites with high wear resistance, *Powder Metall Met Ceram* 2014; 52: 577–587.
27. Mechnik, VA, Effect of hot recompaction parameters on the structure and properties of diamond–(Fe–Cu–Ni–Sn–CrB2) composites, *Powder Metall Met Ceram* 2014; 52: 709–721.
28. Gevorkyan, et al., Peculiarities of obtaining diamond–(Fe–Cu–Ni–Sn) hot pressing, *Funct Mater* 2017; 24: 31–45.
29. ISO 3923-2:1981; Metallic powders - Determination of apparent density - Part 2: Scott volumeter method.
30. ISO 3953:2011; Metallic powders - Determination of tap density.